Mutual Interplay of Light Harvesting and Triplet Sensitizing in a Perylene Bisimide Antenna-Fullerene Dyad

ARTICLE *in* THE JOURNAL OF PHYSICAL CHEMISTRY B · JULY 2010

Impact Factor: 3.3 · DOI: 10.1021/jp1035585 · Source: PubMed

Mutual Interplay of Light Harvesting and Triplet Sensitizing in a Perylene Bisimide Antenna−Fullerene Dyad

Christiane C. Hofmann,[†] Stefan M. Lindner,[‡] Michaela Ruppert,[§] Andreas Hirsch,[§] Saif A. Haque,[∥] Mukundan Thelakkat,[‡] and Jürgen Köhler*,[†]

Department of Experimental Physics IV and BIMF, University of Bayreuth, D-95440 Bayreuth, Germany; Applied Functional Polymers, University of Bayreuth, D-95440 Bayreuth, Germany; Organische Chemie II, Friedrich-Alexander-Universität Erlangen-Nürnberg, 91054 Erlangen, Germany; and Department of Chemistry, Imperial College of Science, Technology and Medicine, London SW72AZ, U.K.

Received: April 20, 2010; Revised Manuscript Received: June 8, 2010

A flexible organic dyad consisting of a perylene bisimide antenna covalently linked to a [60]fullerene has been synthesized and studied by electrochemistry, steady-state spectroscopy, and time-resolved spectroscopy. We found that the energy absorbed by the perylene bisimide is transferred to the fullerene with an efficiency close to 100%. The fullerene in turn undergoes intersystem crossing followed by triplet energy transfer back to the perylene bisimide with an efficiency of at least 20%. Hence the perylene bisimide unit acts as an antenna for the fullerene, i.e., effectively extending the fullerene absorption far into the visible spectral range, while at the same time the fullerene acts as a triplet sensitizer for the perylene bisimide. This has severe consequences for the exploitation of the dye antenna−fullerene concept for light harvesting in solar cells.

Introduction

Light harvesting and the accompanying photoinduced processes such as energy transfer and charge transfer are crucial steps in realizing efficient photovoltaic devices. Especially, the development of new generation solar cells using organic molecules and polymers require the detailed understanding of such elementary processes.[1,2] This is because the main difference between inorganic semiconductors and organic materials concerns the character of the excited state after the absorption of light. In a classical semiconductor, the absorption of a photon creates directly free charge carriers, i.e., electrons and holes, whereas in organic materials the photon generates an exciton, which is often associated with a spatially localized bound electron−hole pair.[2,3] In order to generate an electrical current, the exciton must first dissociate which leads to the following chain of events, each of which has to be optimized for an efficient organic solar cell: light absorption, exciton migration, exciton dissociation, and charge collection at the electrodes.[2,4] However, simultaneous optimization of all these processes leads to conflicting constraints. For example, exciton dissociation is usually achieved in a heterojunction between electron-donor and electron-acceptor materials.[5−9] In order to allow for migration of the exciton to the heterojunction within its finite lifetime, a thin layer of photoactive material is favorable. In contrast, for efficient light absorption a thick photoactive layer would be desirable to increase the number of absorbers. This is the reason why bulk heterojunctions, which are composed of a blend of donor and acceptor materials forming an interpenetrating network, have become a major component in organic solar cell layout.[3,10−12]

Typically, the electronically excited states of an organic compound can be singlet (total electronic spin $S = 0$, spin multiplicity 1) or triplet (total electronic spin $S = 1$, spin multiplicity 3) states. Since in organic molecules the electronic ground state is usually a singlet state, optical excitation results also in an excited singlet state. By intersystem crossing the excitation can be transferred nonradiatively into a triplet state that lies energetically below the excited singlet state. While the migration of singlet excitons is mediated by the long-range Coulomb interaction (at large distances often well approximated by a dipole−dipole interaction) which allows these excitons to move quickly over large distances, the migration of triplet excitons is determined by the exchange interaction which relies on orbital overlap restricting their motions to adjacent sites.[13,14] Similarly, the difference in spin multiplicity between singlet and triplet states has a crucial influence on the respective exciton decay time. The exciton lifetimes in organic materials are typically nanoseconds for spin-allowed singlet−singlet transitions and micro- to milliseconds for spin-forbidden triplet−singlet decays.[3,10−12] In other words, in organic molecules, the absorption of light results in quick short-lived singlet excitons and slow long-lived triplet excitons. Whether the trade-off between fast (slow) migration and short (long) lifetime is in favor for the singlet or triplet excitons to reach the donor−acceptor heterojunction more efficiently depends on the actual system.

Owing to its photophysical properties, C_{60} is a widely used material as electron acceptor in organic solar cells. In particular, its derivative [6,6]phenyl-C_{61}-butyric acid methyl ester (PCBM) has become a key component for the development of highly efficient bulk heterojunction solar cells.[11,15−17] However, a severe drawback of PCBM is its poor absorption strength in the visible spectral region.[18] In order to extend the solar spectrum coverage to achieve better absorption efficiencies, the C_{60} derivatives are often coupled with a dye molecule that acts as a light-harvesting antenna.[19−25] A further advantage of exploiting dye molecules for light-harvesting is that their high molecular extinction coefficient allows to reduce the thickness of the photoactive

* Corresponding author. E-mail: juergen.koehler@uni-bayreuth.de.
[†] Department of Experimental Physics IV and BIMF, University of Bayreuth.
[‡] Applied Functional Polymers, University of Bayreuth.
[§] Friedrich-Alexander-Universität Erlangen-Nürnberg.
[∥] Imperial College of Science, Technology and Medicine.

10.1021/jp1035585
Published on Web 06/28/2010

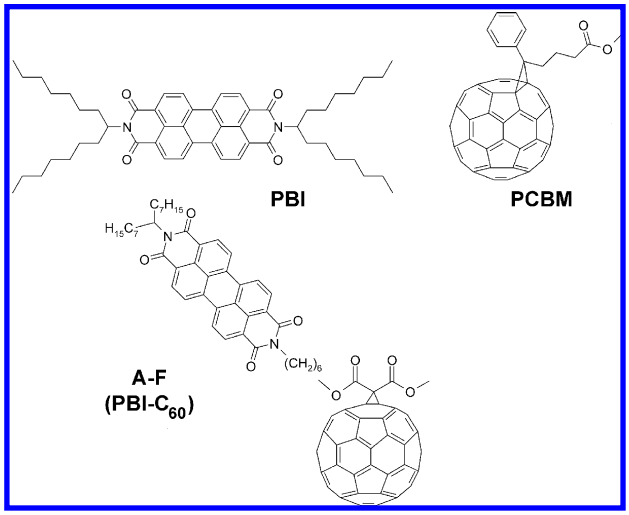

Figure 1. Chemical structures of the investigated compounds. (Top) Chemical structure of the two reference compounds **PBI** (*N*,*N*′-di(1-heptyloctyl)perylene-3,4:9,10-tetracarboxylic bisimide) and **PCBM** ([6,6]phenyl-C_{61}-butyric acid methyl ester). (Bottom) Chemical structure of the dyad **A-F** (PBI−C_{60}).

layer. Even though different dye−C_{60} dyads have been developed with the aim to improve the light-harvesting capabilities and consequently the efficiency of photovoltaic devices, to our knowledge, no such improvement in devices has ever been reported. This is probably due to the complex nature of the transfer processes and the dynamics in such multichromophoric molecules.

Therefore, we want to study the implications on energy and electron transfer processes using such antenna molecules. In particular, we will focus on the photophysical processes between a perylene bisimide (PBI) unit covalently linked to a [60]fullerene in order to shed some light onto the energy and electron transfer processes between these two promising materials. PBI features excellent thermal, photochemical, and photophysical stability as well as strong light absorption in the visible spectral range. Its fluorescence quantum yield is close to 1, testifying that (almost) no excitation energy is lost by other processes.[26−29] Since for PBI also the electron mobility upon optical excitation is high,[30,31] it is unclear whether PBI in combination with C_{60} will act as an energy transfer donor, i.e., a light-harvesting antenna, or whether it will act as an electron transfer donor.

However, in blends, detailed insights of the photophysical properties of organic solar cells at the molecular level are difficult to accomplish. Therefore, donor−acceptor dyads serve often as model systems. In the dyad, the linkage between the PBI and fullerene subunits is a flexible hexyl spacer that allows for a high conformational degree of freedom similar to the situation in polymeric materials. The chemical structure of the PBI−C_{60} dyad is shown in Figure 1, along with the chemical structures of PBI and PCBM that have been studied for reference purposes. In order to keep nomenclature simple, we will refer in the following to the molecules that serve as reference materials as **PBI** and **PCBM**, and to the dyad as **A-F** (A for antenna and F for fullerene), respectively.

Experimental Section

The PBI−C_{60} dyad (**A-F**) was synthesized by coupling C_{60} with the corresponding malonate derivative of PBI (see Supporting Information for synthetic details). **PBI** was prepared according to the literature.[32] **PCBM** was purchased from ADS Inc. All reagents and solvents were of analytical grade or purified using standard methods.

For the cyclic voltammetry experiments a three-electrode assembly with a $Ag/AgNO_3$ electrode was used. The solvent was CH_2Cl_2 containing 0.1 M tetrabutylammonium hexafluorophosphate and each measurement was calibrated with ferrocene as internal standard. All optical spectroscopy experiments were carried out in 10^{-5} M chloroform solution at room temperature. For steady-state spectroscopy, the sample solution was analyzed with commercial spectrometers (absorption, Perkin-Elmer Lambda 9 UV/vis/NIR spectrometer; emission, Varian Cary Eclipse fluorescence spectrophotometer). For the time-resolved fluorescence experiments, the sample was excited with the output of a frequency-doubled pulsed titanium:sapphire laser system (Tsunami, Spectra Physics). The duration of the excitation pulses was 1−2 ps (fwhm) corresponding to a spectral bandwidth of less than 11 cm^{-1} (0.2 nm at 460 nm), respectively. The excitation energy per pulse was varied between 1×10^{-12} and 5×10^{-11} J. The light was focused onto the sample by a fused silica lens, and the polarization of the excitation light was controlled by a half-wave plate. The emission from the sample was collected with an achromatic lens under right angle conditions. The polarization of the detected light was adjusted by a polarization foil. As detector system we used a combination of a spectrograph (250 Imaging Spectrograph, Bruker) and a streak camera (C5680 series, Hamamatsu), providing us with both spectral and time-resolved data featuring a spectral resolution of 3 nm and a temporal resolution of up to 3 ps, depending on the time range of the experiment. In order to exclude polarization anisotropy effects, the fluorescence lifetimes were determined using magic-angle polarization settings between the detected polarization and the polarization of the excitation. The recorded temporal decays were analyzed with commercial software (Fluofit Pro v. 4.1, PicoQuant), using multiexponential fit functions. We employed reconvolution techniques; i.e., the fit function was convoluted with the instrument response, and the result was then compared with the experimental decay curves.

Additionally, we performed microsecond transient absorption experiments. The samples were excited with the output of a dye laser (GL-301, Photon Technology International Inc.) pumped by a pulsed nitrogen laser (GL-3300, Photon Technology International Inc.) emitting pulses of 600 ps duration at 500 nm with a repetition rate of 4 Hz. The pump excitation energy density was between 60 and 80 $\mu J/cm^2$ per pulse. The transient absorption was probed with light from a quartz halogen lamp (IL1, Bentham), that was spectrally discriminated by two monochromators (spectral bandwidth 20 nm) both in the excitation and the detection path. The signal was detected with a silicon photodiode with minimum time increments of 4 ns. More details about this setup can be found elsewhere.[33]

Results

Cyclovoltammetry. The electrochemical properties of **A-F** were determined by cyclic voltammetry and compared with those of the reference compounds **PBI** and **PCBM**. The measurements were conducted on a glassy carbon working electrode coupled with a $Ag/AgNO_3$ reference electrode and a Pt counter electrode in a three-electrode assembly system using CH_2Cl_2 containing 0.1 M tetrabutylammonium hexafluorophosphate as solvent. The HOMO (highest occupied molecular orbital) and LUMO (lowest unoccupied molecular orbital) values were calculated with respect to ferrocene (HOMO −4.8 eV). It could be shown that **PBI** exhibits two reversible reduction peaks

TABLE 1: Cyclovoltammetry Data for the Compounds PBI, PCBM, and the Dyad A-F[a]

compound	reduction peak voltages		
PBI	−1.09	−1.29	−
PCBM	−1.11	−	−1.49
A-F	−1.09	−1.28	−1.45

[a] The reduction potentials are given in volts with respect to ferrocene.

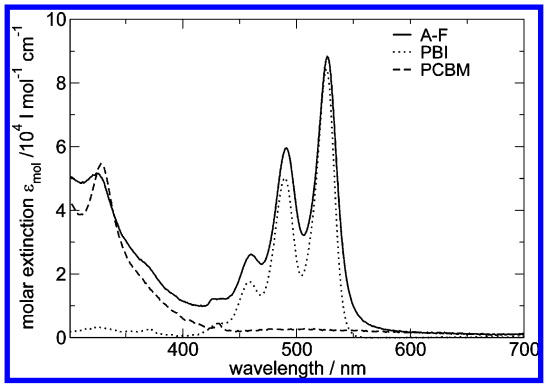

Figure 2. Steady-state absorption spectra of the dyad **A-F** (solid line) and the reference compounds **PBI** (dotted line) and **PCBM** (dashed line) in 10^{-5} M chloroform solution.

at −1.09 and −1.29 V and one oxidation peak at +1.23 V. The LUMO value was calculated from the first reduction E_{red1} as −3.71 eV and the HOMO from the first oxidation peak E_{ox1} as −6.03 eV with respect to the zero energy level. The fullerene derivative **PCBM** also shows two reversible reduction peaks, at −1.11 and −1.49 V, and an irreversible oxidation peak. The first reduction potential of **PCBM** is comparable to the first reduction potential of **PBI**. Yet the second reduction peaks of **PBI** and **PCBM** occur at different potentials. Consequently, three reduction peaks appear for the dyad **A-F**, the first of which is an overlap of the first reduction peaks of the fullerene and perylene bisimide units. The second and third reduction peaks of the dyad occur at similar potential values as the second reduction peaks of the individual compounds. The reduction peak voltages are summarized in Table 1.

Steady-State Spectroscopy. ***Absorption Spectra.*** The absorption spectra of **PBI**, **PCBM**, and the dyad **A-F** are shown in Figure 2. The **PBI** absorption maximum is located at 526 nm and is accompanied by a vibronic progression peaking at 490 and 459 nm, respectively. The peak optical density at 526 nm corresponds to a molar extinction of 84 000 L mol^{-1} cm^{-1}. The molar extinctions for the 490 and 459 nm absorption maxima are 50 000 and 17 000 L mol^{-1} cm^{-1}, respectively. Between 300 and 450 nm, the **PBI** absorbance decreases, but remains on a finite level (1700 L mol^{-1} cm^{-1} at 350 nm). These values are in agreement with earlier publications; cf., e.g., refs 34−38. **PCBM** shows a weak, featureless absorption over the whole visible spectral range (2400 L mol^{-1} cm^{-1} at 460 nm). A close look at the red edge of the absorption spectrum uncovers the spectral origin (data not shown) at 696 ± 2 nm.[18,39] In the UV, we find an absorption maximum at 328 nm (54 000 L mol^{-1} cm^{-1}), which reflects the absorption of higher-lying electronic states.[18,39]

The absorption spectrum of the dyad **A-F** features bands at essentially the same spectral positions as observed for its constituents. However, we find differences regarding the extinctions of these bands. The absorption maximum that can be associated with the **F** unit is blue-shifted to 324 nm and features

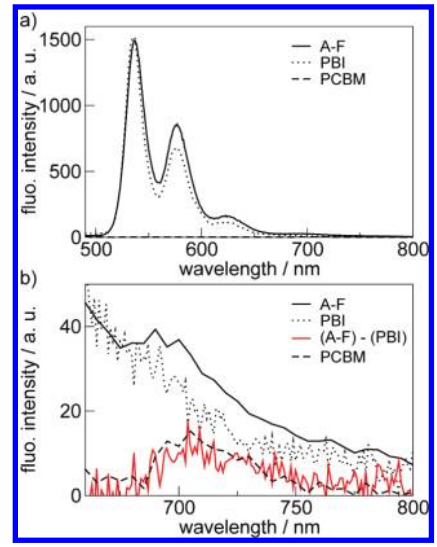

Figure 3. (a) Steady-state emission spectra of the dyad **A-F** (solid line) and the reference compounds **PBI** (dotted line) and **PCBM** (dashed line) in 10^{-5} M chloroform solution, for the excitation wavelength λ_{ex} = 460 nm. The total intensity of the dyad emission decreases to about 1.9% as compared to the total emission intensity of **PBI**. Therefore, for better comparison, the spectra for **A-F** and **PBI** have been normalized. (b) NIR part of the steady-state emission of **A-F** upon excitation of the **A** moiety at 460 nm (black full line). The dotted line corresponds to a **PBI** emission spectrum that has been scaled by a factor of 0.037 to match the intensity of the **A-F** emission between 660 and 680 nm. The red line represents the difference between the **A-F** emission and the scaled **PBI** emission. For comparison, the dashed line shows the **PCBM** emission spectrum, excited at the same wavelength, which has been multiplied by a factor of 5.

an extinction of 51 000 L mol^{-1} cm^{-1}, which is about 94% of the value found for isolated **PCBM**. With respect to the **A**-associated absorption bands, we find the absorption maximum slightly red-shifted at 527 nm. The maxima of the vibronic progression are found at 491 and 460 nm. For the extinction of **A-F** at the absorption maximum we obtain 88 000 L mol^{-1} cm^{-1}, which corresponds to about 105% of the extinction of isolated **PBI**. Comparison of the vibronic progression peaks yields a value of 1.7 for the ratio of the extinctions of the first and second vibronic peak for **PBI**, whereas this value decreased to 1.5 for **A-F**.

Emission Spectra. The emission spectra of **PBI**, **PCBM**, and the dyad **A-F** are shown in Figure 3 for the excitation wavelength 460 nm. Excitation at 460 nm yields for **PBI** the well-known emission spectrum with maxima at 535 and 576 nm, and a shoulder at 624 nm, whereas for isolated **PCBM** only an extremely weak emission maximum around 700 nm can be detected. These spectra are in agreement with published data (cf., e.g., refs 18 and 34−38).

For this excitation wavelength, we find for the dyad almost exclusively an emission from the **A** moiety. It features maxima at 537 and 577 nm, and a shoulder around 624 nm. The ratio of the intensities of the maxima of the first and the second vibronic peak decreases from 2.2 in **PBI** to 1.7 in **A-F**. While the overall shape of the emission spectrum of **A-F** resembles that of **PBI**, the total emission intensity of **A-F** corresponds only to about 1.9% of the total emission intensity of isolated **PBI**. Yet, additionally, we find for **A-F** a weak maximum around 700 nm on top of the red wing of the emission of the **A** subunit that we consider in more detail in Figure 3b. In order to account for the background from the **A** emission, we subtracted the emission of the **PBI** reference. However, since both the total emission intensity and the ratios of the intensities of the vibronic

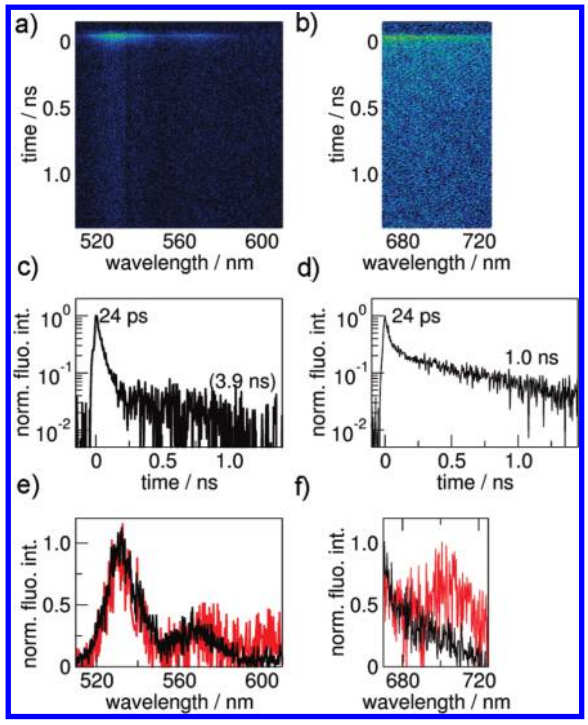

Figure 4. Temporally and spectrally resolved emission of the dyad for a 10^{-5} M solution in chloroform excited at 460 nm. Streak camera images for (a) 510−610 nm and (b) 670−725 nm. The horizontal axis corresponds to wavelength, the vertical axis corresponds to time, and the detected intensity is given by the color scale, where blue represents low intensity and red represents high intensity. (c and d) Fluorescence decay curves obtained by integration of the streak data along the wavelength axis in the spectral regions shown in (a) and (b), respectively. (e and f) Time-resolved emission spectra obtained by integration of the streak image along the time axis. The black curves correspond to the emission accumulated during the first 30 ps after excitation, and the red curves represent the emission accumulated during the interval 30−530 ps after the excitation.

progression of the **PBI** reference deviate from the emission of the **A** subunit, we followed a pragmatic approach and scaled the **PBI** reference spectrum such that it matched the intensity of the **A-F** emission between 660 and 680 nm (Figure 3b, dotted line). From this procedure, we obtained the red curve in Figure 3b which features a maximum at 705 ± 5 nm with a width of 60 nm (fwhm). The shape of the difference spectrum resembles the **PCBM** emission, excited at the same wavelength, which is shown by the dashed line in Figure 3b.

Time-Resolved Fluorescence Spectroscopy. In Figure 4 we show an example of the experimental results obtained with the streak camera for the **A-F** sample upon excitation at 460 nm. The spectral regions of the emission can be associated with the **A** (left-hand side) and the **F** subunit (right-hand side) within the dyad, respectively. Figure 4a displays the streak image, i.e., the time-resolved emission spectrum, of the dyad. The horizontal axis corresponds to the emission wavelength and runs from 510 to 610 nm, while the vertical axis corresponds to time and covers an interval of 1.5 ns length after the excitation pulse. The detected emission intensity is given by the color scale. Integration of the streak image along the wavelength axis from 510 to 610 nm yields the fluorescence decay curve that is shown in Figure 4c on a semilogarithmic scale. The decay is clearly not monoexponential and features a short and a long lifetime component. In order to determine these lifetimes with better accuracy, the streak experiment was repeated in time windows of 200 ps and 50 ns, respectively. From a biexponential fit to the data, we find for the short component a lifetime of τ_{short} = 24 ± 3 ps and a relative amplitude A_{short} = 0.97. For the long component we find τ_{long} = 3.9 ± 0.3 ns and A_{long} = 0.03. The long decay time matches the lifetime of **PBI**, which was determined to 3.8 ± 0.2 ns in the same solvent. Finally, Figure 4e shows the time-resolved emission spectra that are obtained by integrating the streak image along the time axis either for the first 30 ps after excitation (black curve) or for the time interval from 30 to 530 ps after excitation (red curve). Both spectra appear to be similar and resemble the emission spectrum of the **PBI** reference.

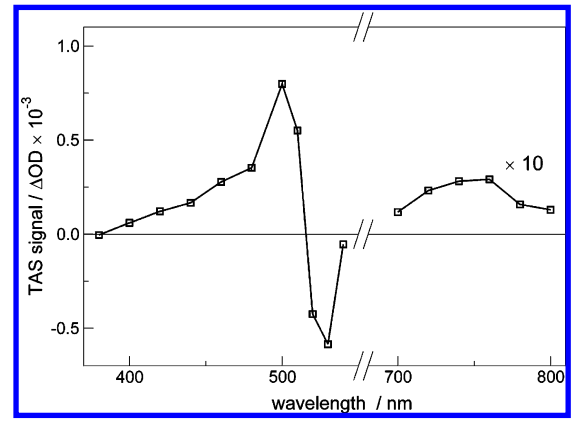

Figure 5. Transient absorption spectrum (TAS) of **A-F** for a 10^{-5} M solution in chloroform. The transient absorption signals were probed 0.5 μs after pulsed excitation at 500 nm. The squares represent the measured transient spectrum. The lines serve as a guide for the eye.

The spectral region covered on the right-hand side of Figure 4 can be associated with the **F** subunit in the dyad. The wavelength axis of the streak image (Figure 4b) runs from 680 to 720 nm and the time interval covered after the pulse is again 1.5 ns. Integration of the streak image along the wavelength axis from 675 to 710 nm yields the decay curve shown in Figure 4d. The decay is again compatible with a biexponential fit, with the parameters τ_{short} = 24 ± 10 ps, A_{short} = 0.79, and τ_{long} = 1.0 ± 0.3 ns, A_{long} = 0.21. The relatively large errors of the lifetimes are due to the weak fluorescence signal in that spectral region. Nevertheless, the lifetime of the long component is in close agreement with the fluorescence lifetime of the **PCBM** reference which was determined to 0.9 ± 0.3 ns. The time-resolved emission spectrum accumulated during the first 30 ps after the excitation shows the low-energy wing (Figure 4f, black line) that can be associated with the emission from the **A** subunit. Yet, the fluorescence emitted between 30 and 530 ps after the excitation shows a clear maximum around 700 nm (Figure 4f, red curve) and agrees with the **F**-associated emission profile; see Figure 3b.

Transient Absorption Spectroscopy. The transient absorption spectrum of a 10^{-5} M solution of **A-F** in chloroform, probed 0.5 μs after pulsed excitation at 500 nm, is shown in Figure 5. We find a positive transient absorption signal between 400 and 510 nm with a well-defined maximum around 500 nm. At wavelengths longer than 515 nm, the dyad shows negative transient absorption, with a well-defined minimum around 530 nm, reflecting the ground-state bleaching of the **A** subunit. In the spectral region between 700 and 800 nm, the transient absorption spectrum of **A-F** shows a weak positive signal with a maximum around 760 nm. This signal is about a factor of 30 weaker with respect to the signal around 500 nm. All transient absorption signals featured decay time constants comparable to the instrument response of 10^{-7} s.

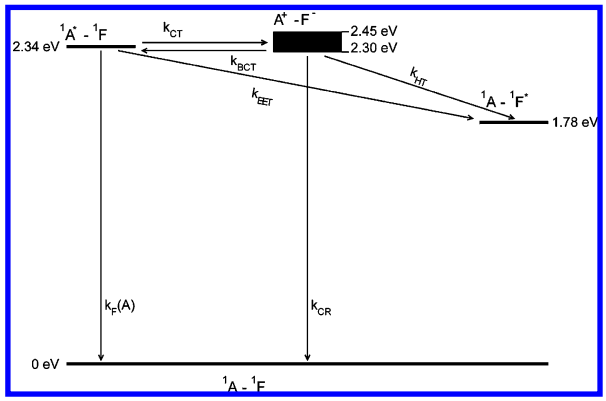

Figure 6. Free energy differences of the electronic states of the dyad **A-F** (relative to the ground state) and rates for various photophysical processes. $k_F(A)$ corresponds to the decay rate of the A-associated excited state to the ground state; k_{EET} describes the singlet excitation energy transfer; k_{CT} is the rate for forward electron transfer; k_{BCT} describes back electron transfer; k_{CR} is the rate for charge recombination to the ground state; and k_{HT} is the rate for a ground-state charge transfer resulting in a neutral state with an excitation localized on the fullerene **F** (ground-state hole transfer from A^+ to F^-). The ambiguity for the energetic position of the charge separated state, A^+-F^-, due to the different possible conformations of the dyad, is indicated by the black area, where the top refers to a fully stretched geometry and the bottom refers to a folded dyad.

Discussion

On first sight, the profiles of the absorption and emission spectra of the dyad **A-F** resemble the sums of the respective spectra from the reference compounds. Yet, for the **A-F** emission spectrum, excited at 460 nm, two significant deviations from the reference spectra can be found. First, the band around 700 nm, which can be associated with the **F** moiety, is about 5 times as strong in intensity with respect to the **PCBM** emission excited at the same wavelength, and, second, the total intensity of the dyad emission decreases to about 1.9% as compared to the total emission intensity of **PBI**. The first observation already provides experimental evidence for an excitation energy transfer from the **A** to the **F** subunit in the dyad. A coarse estimate for the energy transfer efficiency can be obtained from the enhancement factor of the **F**-associated emission in the dyad and the absorption strengths of the reference compounds. If we assume that the molar absorption strength at 460 nm for **PCBM** and for C_{60} within the dyad, i.e., the **F** subunit, has not changed significantly, then 4/5 of the intensity of the **F**-associated emission results from energy transfer from the **A** subunit. Hence, $\eta_{EET} = 4\varepsilon_{PCBM}/\varepsilon_{PBI}$. Inserting the molar extinctions at 460 nm as $\varepsilon_{PCBM} = 2400$ L mol^{-1} cm^{-1} and $\varepsilon_{PBI} = 17\,000$ L mol^{-1} cm^{-1} yields $\eta_{EET} = 0.6 \pm 0.4$.

However, from the steady-state data, no information can be gained whether further photophysical processes, as summarized in Figure 6, are effective as well. Excitation into the **A**-moiety of the dyad results in a state $^1A^*-{}^1F$, where the asterisk refers to an electronically excited singlet state located on **A** while **F** remains in the electronic ground state. The excitation can decay directly back to the ground state with a rate $k_F(A)$ or it can be transferred with a rate k_{EET} to the **F** moiety resulting in the state $^1A-{}^1F^*$. Intersystem crossing of **A** into the excited triplet state is neglected because it is known that for perylene bisimides and its derivatives the quantum yield for this process is extremely low.[26,28,29,34,40] An examination of the oxidation and reduction potentials of the **F** and **A** subunits precludes the possibility of a charge transfer process leading to a charge-separated state A^--F^+. However, it is known as well[15,30] that **PBI** is an efficient electron donor and that C_{60} acts as a strong electron acceptor. Therefore, charge transfer processes (here electron transfer) leading to a charge-separated state A^+-F^- cannot be excluded beforehand. This state can be depleted by ground-state charge transfer (hole transfer, rate k_{HT}) leading also to the formation of the state $^1A-{}^1F^*$, or it can decay by charge recombination with a rate k_{CR}. In order to discuss the relevance of the various processes, the differences in free energy between the involved electronic states are required. From the intersections of the absorption and emission spectra of the reference compounds, the $(^1A^*-{}^1F) \leftarrow (^1A-{}^1F)$ and $(^1A-{}^1F^*) \leftarrow (^1A-{}^1F)$ energies were determined to be 2.34 ± 0.01 and 1.78 ± 0.01 eV above the electronic ground state, which was set to zero energy as reference point. The energy of the charge-separated state, A^+-F^-, depends on the change of the free energy ΔG_{CT} upon electron transfer with respect to the energy ΔG^0 of the state $^1A^*-{}^1F$. This is given as[41,42]

$$\Delta G_{CT} = (E_{ox} - E_{red}) + \frac{e^2}{4\pi\varepsilon_0}\left[\frac{1}{2}\left(\frac{1}{r^+} + \frac{1}{r^-}\right)\left(\frac{1}{\varepsilon} - \frac{1}{\varepsilon_{ref}}\right) - \frac{1}{\varepsilon}\frac{1}{d}\right] - \Delta G^0((^1A^*-{}^1F) \leftarrow (^1A-{}^1F)) \quad (1)$$

The first term describes the difference between the oxidation and reduction potentials of the dyad which have been determined by cyclovoltammetry (in dichloromethane) to $E_{ox} = 1.23$ eV and $E_{red} = -1.09$ eV. The second term takes into account that the optical experiments and the cyclovoltammetry have been carried out in different solvents. Here ε and ε_{ref} are the dielectric constants of chloroform and dichloromethane. r^+ and r^- refer to the electronic radii of the cation and the anion and have been estimated as 0.55 nm for A^+[43] and 0.44 nm for F^-.[24] Finally, d corresponds to the center-to-center distance of the chromophores. Since the linker between the **A** and **F** subunits is a flexible carbon chain, d can cover the range from $d_{min} \approx r^+ + r^- = 1.0$ nm for a completely folded dyad to $d_{max} \approx 2.0$ nm for a fully stretched dyad. From these numbers, we find for an excited-state electron transfer a change of the free energy ΔG_{CT} between -0.04 eV (for the folded conformation) and 0.11 eV (for the fully stretched conformation) with respect to the neutral electronically excited state $^1A^*-{}^1F$. The energies of the various electronic states of the dyad are reproduced as well in Figure 6, where the range that is covered by the charge-separated state is indicated by the black box. From Figure 6 the following kinetic model is deduced:

$$\frac{d}{dt}((^1A^*-{}^1F)(t)) = (-k_F(A) - k_{EET} - k_{CT})(^1A^* - {}^1F)(t) + k_{BCT}(A^+ - F^-)(t) \quad (2)$$

$$\frac{d}{dt}((A^+ - F^-)(t)) = k_{CT}(^1A^* - {}^1F)(t) + (-k_{BCT} - k_{HT} - k_{CR})(A^+ - F^-)(t) \quad (3)$$

$$\frac{d}{dt}((^1A - {}^1F^*)(t)) = k_{EET}(^1A^* - {}^1F)(t) + k_{HT}(A^+ - F^-)(t) - k(F)(^1A - {}^1F^*)(t) \quad (4)$$

In addition to the rates that have been detailed already in the context of Figure 6, we have introduced a general rate $k(F)$ that takes the depletion of the state $^1A-{}^1F^*$ into account. But even when we use the approximations $k_F(A) \approx 1/\tau_{PBI}$ and $k(F) \approx$

TABLE 2: Free Energy Differences ΔG^0 and Rates for Different Electron-Transfer Processes, Evaluated According to the Marcus−Jortner Formalism Given in Eq 5 for a Distance $d = 1.0$ nm between A and F (Folded Dyad)[a]

	ΔG^0 (eV)	rate (s^{-1})
k_{CT}	−0.04	$3.00 \times 10^{14} \times V^2$
k_{BCT}	0.04	$6.49 \times 10^{13} \times V^2$
k_{HT}	−0.52	$1.48 \times 10^{16} \times V^2$
k_{CR}	−2.30	$1.32 \times 10^{11} \times V^2$

[a] V is the electronic coupling for each process and is given in eV. Generally, V depends on the states between which the transition takes place.

$1/\tau_{PCBM}$, by exploiting the lifetimes observed for the references, we are still left with five unknown parameters, i.e., the rate of excitation energy transfer k_{EET}, and the four charge-transfer rates. Therefore, we followed the formalism of Marcus and Jortner which allows to calculate the charge transfer rates by treating electron transfer as an activated process including vibrational coupling. This approach provides reasonable results as has been shown in particular for organic dyads.[44] Accordingly, the rate k of an electron transfer process is expressed as a function of the free energy difference ΔG^0 between the initial and the final state, the reorganization energy λ, and the electronic coupling V between the two states[44−49]

$$k = \left(\frac{4\pi^3}{h^2\lambda_S k_{BT}}\right)^{1/2} V^2 e^{-S} \sum_{j=0}^{\infty} \left[\frac{S^j}{j!} \exp\left(-\frac{(\Delta G^0 + \lambda_S + jh\nu)^2}{4\lambda_S k_B T}\right)\right] \quad (5)$$

Here k_B denotes the Boltzmann constant, h the Planck constant, T the temperature, S the Huang−Rhys factor, j the vibrational quantum number, and ν the vibrational frequency. The reorganization energy $\lambda = \lambda_i + \lambda_S$ has been separated into an internal part $\lambda_i = Sh\nu$ and a part λ_S that relates to the solvent. For the calculations we have used $h\nu = 0.186$ eV, which corresponds to a vibrational frequency of 1500 cm^{-1}, a typical value for a carbon−carbon double bond stretch vibration in aromatic systems.[26,43,44] For λ_i, we used the value for **PBI**, $\lambda_i \approx 0.25$ eV,[26,43,44] because λ_i has been reported as relatively small for C_{60}.[50,51] Hence, we obtain a Huang−Rhys factor $S = 1.34$ for the effective mode vibrational coupling. The solvent reorganization energy can be obtained from

$$\lambda_S = \frac{e^2}{4\pi\varepsilon_0}\left[\frac{1}{2}\left(\frac{1}{r^+} + \frac{1}{r^-}\right) - \frac{1}{d}\right]\left(\frac{1}{n^2} - \frac{1}{\varepsilon}\right) \quad (6)$$

where n represents the refractive index of the solvent, and r^+, r^-, d, and ε are defined as above. The ΔG^0 values for the different charge-transfer processes correspond to the free energy differences between the initial and final states as given in Figure 6 and are summarized in Table 2 together with the calculated charge transfer rates (for an interchromophoric distance $d =$ 1.0 nm, i.e., a folded dyad). The explicit value of V^2 has not been specified yet. On the basis of the results in ref 44, we treat the electronic coupling V as a constant irrespective of the initial and final states involved. Hence, the only unknown parameters left in the rate eqs 2−4 are the electronic coupling V and the energy transfer rate k_{EET}. The general solution of eqs 2−4 is of the form

$$({}^1A^*-{}^1F)(t) = \alpha_1 \exp(-\kappa_1 t) + \alpha_2 \exp(-\kappa_2 t) \quad (7)$$

$$(A^+ - F^-)(t) = \beta_1 \exp(-\kappa_1 t) + \beta_2 \exp(-\kappa_2 t) \quad (8)$$

$$({}^1A - {}^1F^*)(t) = \gamma_1 \exp(-\kappa_1 t) + \gamma_2 \exp(-\kappa_2 t) + \gamma_3 \times \exp(-\kappa_3 t) \quad (9)$$

with the rate eigenvalues κ_i ($i = 1,2,3$) and the amplitudes α_i, β_i, and γ_i, respectively, which can be expressed as functions of the unknown parameters. Tentatively, we assign the three experimentally observed decay times to the inverse of the rate eigenvalues $\kappa_1 = (24\text{ ps})^{-1}$, $\kappa_2 = (3.9\text{ ns})^{-1}$, and $\kappa_3 = (1.0\text{ ns})^{-1}$. Solving the eqs 2−4 yields $k_{EET} = 4.1 \times 10^{10}$ s^{-1} and $V = 0.13$ meV for the folded conformation. The association of the experimental lifetimes with the rate eigenvalues can be controlled by calculating the ratio of the relative amplitudes of the fast and the slow decay component of the **A**-associated fluorescence giving $\alpha_2/(\alpha_2 + \alpha_1) \approx 10^{-8}$ in striking contrast with the value of 0.03 that was found experimentally. A way out of this puzzle is provided by the fact that the lifetime of 3.9 ns is in close agreement with the decay time of isolated **PBI** and might stem from impurities rather than being related to processes in the dyad.[25] Intermediates from the chemical synthesis featuring similar fluorescence characteristics as **PBI** might be responsible for this discrepancy. Hence we disregard the assignment $\kappa_2 = (3.9\text{ ns})^{-1}$ and treat κ_2 as unknown.

In order to deal with this reservation, we tested the variation of k_{EET} and V as a function of κ_2 which was varied from $(25\text{ ps})^{-1}$ as a lower limit to $(1\ \mu s)^{-1}$ as maximum value. For the energy transfer rate we found that the calculated value of $k_{EET} = 4.1 \times 10^{10}$ s^{-1} showed only minor variations of less than 0.5% as a function of the input value for κ_2. For the coupling constant V we found values between 8.2 μeV, for $\kappa_2 = (1\ \mu s)^{-1}$, and 1.6 meV, for $\kappa_2 = (25\text{ ps})^{-1}$. From the most extreme choice of these numbers, the maximum electron-transfer rate that can be obtained is $k_{CT} = 7.7 \times 10^8$ s^{-1} which is only 2% of the energy transfer rate k_{EET}. This allows us to calculate the energy transfer efficiency from **A** to **F** more accurately: $\eta_{EET} = k_{EET}/(k_F(A) + k_{EET} + k_{CT}) \geq 0.98$.

So far, we have neither considered the influence of the conformation of the dyad nor the polarity of the solvent on the character of the photophysical processes within the dyad. All calculations of the rate constants have been performed for a completely folded dyad. Yet, any deviation from this geometry will lead to an increase of the distance between the chromophores and charge-transfer processes become even less favorable. The other issue concerns the question whether charge-transfer processes might become more favorable over energy-transfer processes in solvents with higher polarity. Clearly, for more polar solvents than chloroform the difference in free energy between the excited state ${}^1A^*-{}^1F$ and the charge-separated state A^+-F^- will be increased. However, in a more polar solvent the reorganization energy will be increased as well. The mutual influence of these two effects on the charge-transfer dynamics can be tested by inserting the dielectric constants and refractive indices for solvents of different polarity into eqs 5 and 6. This yields that the rate k_{CT} can be increased by at most 1 order of magnitude upon changing the solvent from chloroform ($\varepsilon =$ 4.8, $n = 1.46$) to solvents with high dielectric constants and refractive indices, e.g., nitrobenzene ($\varepsilon = 34.8$, $n = 1.56$, $k_{CT} = 6.3k_{CT}(CHCl_3)$). For this example solvent, this yields a corresponding reduction of the energy transfer efficiency to

about $\eta_{EET} \geq 89\%$. Nevertheless, we can state that an electronic excitation that is initially located on the **A** subunit decays predominantly by excitation energy transfer to the **F** subunit.

The lifetime of the **F**-associated emission is in close agreement with the value found for C_{60}, which is known to undergo intersystem crossing to the triplet state with a quantum yield of nearly 100%.[52−56] A fingerprint for the population of the triplet state of **PCBM** would be a transient absorption signal around 720 nm (obtained for **PCBM** in argon degassed toluene[25]). For the dyad **A-F** we observe only a weak transient absorption signal around 760 nm and it is not clear whether this signal can be attributed to the triplet state of the **F**-subunit. But at any rate these data testify that no significant population is accumulated in the triplet state of the **F** moiety. Instead, we find a strong transient absorption signal around 500 nm which is consistent with the triplet−triplet absorption of perylene bisimide.[26,34] Since perylene bisimide has a very low triplet yield, we exclude a population of this state by intersystem crossing from the $^1A^*-{}^1F$ state. In agreement with the fact that we do not observe the buildup of a significant triplet population of the **F** moiety, we propose that the triplet state of the **A** subunit is populated by triplet−triplet energy transfer from the **F** triplet state. This is reasonable, because the energies of the triplet states of the fullerene and perylene bisimide compounds are reported to be 1.50[57] and 1.2 eV,[26,34] respectively. A lower boundary for the triplet−triplet energy transfer efficiency η_{TEET} can be obtained from the transient absorption of the **A** triplet state, ΔOD, by

$$\eta_{TEET} = \Delta OD/(\eta_{exc}\eta_{EET}\eta_{ISC}(F)\varepsilon_{3A}cl) \qquad (10)$$

Here, $\eta_{EET} = 0.98$ corresponds to the efficiency of the singlet−singlet energy transfer from **A** to **F**, and $\eta_{ISC}(F)$ represents the intersystem crossing efficiency of the **F** moiety to the triplet state which we have approximated as $\eta_{ISC}(F) = 1$.[52−56] The molar extinction of the **A** triplet−triplet absorption is given by $\varepsilon_{3A} = 6 \times 10^4$ L mol^{-1} cm^{-1} where we have used the value reported for **PBI**.[26,34] For the dyad concentration we used $c = 10^{-5}$ M and for the cuvette length $l = 1$ cm. Finally, η_{exc} denotes the excitation efficiency which is given by the number of photons absorbed per pump pulse as

$$\eta_{exc} = \frac{1}{3}\frac{\ln 10\varepsilon_{A-F}}{N_A}\frac{\lambda}{hc_0}\phi \qquad (11)$$

where $\varepsilon_{A\text{-}F}$ corresponds to the molar extinction of the dyad at 500 nm, N_A is Avogadro's number, c_0 is the speed of light in vacuum, and $\phi \approx 70$ μJ/cm^2 is the energy density of the pump laser. The factor 1/3 accounts for the fact that we excited the randomly oriented molecules with linearly polarized light. From these numbers, we obtain $\eta_{exc} \approx 0.006$ and subsequently for the triplet−triplet energy transfer efficiency $\eta_{TEET} \approx 0.2$ where we have used the measured value of $\Delta OD = 8 \times 10^{-4}$ at 500 nm. Given the fact that the triplet lifetime could not be resolved in the transient absorption experiment, the value for the triplet−triplet energy transfer efficiency should be treated as a lower boundary.

Since triplet−triplet energy transfer is governed by short-range exchange interactions, it plays only a role for intermolecular distances of 10 Å or less.[13] The measurable triplet energy-transfer efficiency that we found for **A-F** is thus an indication that a folded conformation with a center-to-center distance close to 10 Å prevails. Given the flexibility of the $(CH_2)_6$ bridge and the $\pi-\pi$ interactions between the **A** and **F** moieties, this appears reasonable.

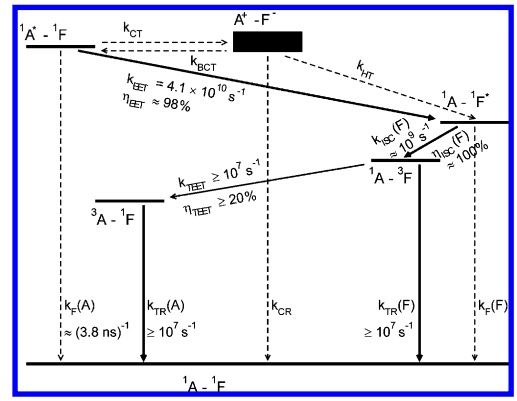

Figure 7. Photophysical processes upon electronic excitation of the **A** subunit into the first excited singlet state. The dominating pathways are indicated by thick arrows, and minor decay pathways are indicated by broken arrows. The rates $k_F(A)$, k_{EET}, k_{CT}, k_{BCT}, k_{CR}, and k_{HT} are defined as in Figure 6. $k_{ISC}(F)$ is the rate for intersystem crossing on the **F** subunit and k_{TEET} represents triplet−triplet energy transfer. $k_F(F)$ represents the decay rate of the singlet state on the **F** subunit to the electronic ground state. The rates $k_{TR}(A)$ and $k_{TR}(F)$ indicate a transition from the localized triplet states on the **A** or **F** moieties, respectively, to the ground state.

In Figure 7 we have summarized the sequence of photophysical processes upon electronic excitation of the first excited singlet state of the **A** subunit within the dyad **A-F**. The rates and efficiencies of the respective processes as deduced from our data are also included in Figure 7. In the dyad the first excited singlet state of the **A** moiety decays predominantly by energy transfer to the first excited singlet state of the **F** subunit. For chloroform as a solvent, the efficiency of this process is at least 98% and the formation of a charge-separated state A^+-F^- as an intermediate can be neglected. The population in the singlet state of the **F** manifold is transferred by intersystem crossing to the **F** triplet state with an efficiency close to 100%, and subsequently by triplet−triplet energy transfer back to the **A** subunit. The latter process occurs with an efficiency of at least 20%.

Conclusions

We have elucidated a detailed description of the photophysical processes that occur in a dyad consisting of a perylene bisimide chromophore covalently linked to C_{60}. We observed an efficient transfer of the electronic excitation energy form the perylene bisimide to the fullerene followed by a back-transfer of the excitation energy from the fullerene to the triplet state of the perylene bisimide. The charge-transfer processes from the excited state of the perylene bisimide to the fullerene play only a minor role. If one succeeds in funneling the excitation energy from the fullerene to another building block prior to intersystem crossing within the fullerene, the perylene bisimide indeed has the potential to act as an effective antenna to extend the fullerene absorption into the visible spectral region. Yet, the fullerene could also be exploited as a triplet sensitizer for the perylene bisimide which features only a negligible intersystem crossing yield.

Acknowledgment. C.C.H. gratefully acknowledges support from the Elite Network of Bavaria (ENB) program "Macromolecular Science" and the ENB scholarship program as well as support from the European Science Foundation (ESF) activity "New Generation of Organic Based Photovoltaic Devices".

Supporting Information Available: Synthesis of the dyad **A**-**F**. This material is available free of charge via the Internet at http://pubs.acs.org.

References and Notes

(1) Wasielewski, M. R. Energy, Charge, and Spin Transport in Molecules and Self-Assembled Nanostructures Inspired by Photosynthesis. *J. Org. Chem.* **2006**, *71*, 5051–5066.

(2) Brédas, J.-L.; Norton, J. E.; Cornil, J.; Coropceanu, V. Molecular Understanding of Organic Solar Cells: The Challenges. *Acc. Chem. Res.* **2009**, *42*, 1691–1699.

(3) Roncali, J. Molecular Bulk Heterojunctions: An Emerging Approach to Organic Solar Cells. *Acc. Chem. Res.* **2009**, *42*, 1719–1730.

(4) Peumans, P.; Uchida, S.; Forrest, S. R. Efficient Bulk Heterojunction Photovoltaic Cells Using Small-Molecular-Weight Organic Thin Films. *Nature* **2003**, *425*, 158–162.

(5) Tang, C. W. 2-Layer Organic Photovoltaic Cell. *Appl. Phys. Lett.* **1986**, *48*, 183–185.

(6) Peumans, P.; Yakimov, A.; Forrest, S. R. Small Molecular Weight Organic Thin-Film Photodetectors and Solar Cells. *J. Appl. Phys.* **2003**, *93*, 3693–3723.

(7) Bach, U.; Lupo, D.; Comte, P.; Moser, J. E.; Weissortel, F.; Salbeck, J.; Spreitzer, H.; Grätzel, M. Solid-State Dye-Sensitized Mesoporous TiO_2 Solar Cells with High Photon-to-Electron Conversion Efficiencies. *Nature* **1998**, *395*, 583–585.

(8) Handa, S.; Wietasch, H.; Thelakkat, M.; Durrant, J. R.; Haque, S. A. Reducing Charge Recombination Losses in Solid State Dye Sensitized Solar Cells: The Use of Donor-Acceptor Sensitizer Dyes. *Chem. Commun.* **2007**, 1725–1727.

(9) Karthikeyan, Ch. S.; Wietasch, H.; Thelakkat, M. Highly Efficient Solid-State Dye-Sensitized TiO_2 Solar Cells Using Donor-Antenna Dyes Capable of Multistep Charge-Transfer Cascades. *Adv. Mater.* **2007**, *19*, 1091–1095.

(10) Sariciftci, N. S.; Smilowitz, L.; Heeger, A. J.; Wudl, F. Photoinduced Electron-Transfer from a Conducting Polymer to Buckminsterfullerene. *Science* **1992**, *258*, 1474–1476.

(11) Ma, W.; Yang, C.; Gong, X.; Lee, K.; Heeger, A. J. Thermally Stable, Efficient Polymer Solar Cells with Nanoscale Control of the Interpenetrating Network Morphology. *Adv. Funct. Mater.* **2005**, *15*, 1617–1622.

(12) Thompson, B. C.; Fréchet, J. M. Organic Photovoltaics - Polymer-Fullerene Composite Solar Cells. *Angew. Chem., Int. Ed.* **2008**, *47*, 58–77.

(13) Scholes, G. D. Long-Range Resonance Energy Transfer in Molecular Systems. *Annu. Rev. Phys. Chem.* **2003**, *54*, 57–87.

(14) Speiser, S. Photophysics and Mechanisms of Intramolecular Electronic Energy Transfer in Bichromophoric Molecular Systems: Solution and Supersonic Jet Studies. *Chem. Rev.* **1996**, *96*, 1953–1976.

(15) Yu, G.; Gao, J.; Hummelen, J. C.; Wudl, F.; Heeger, A. J. Polymer Photovoltaic Cells−Enhanced Efficiencies via a Network of Internal Donor-Acceptor Heterojunctions. *Science* **1995**, *270*, 1789–1791.

(16) Hummelen, J. C.; Knight, B. W.; LePeq, F.; Wudl, F.; Yao, J.; Wilkins, C. L. Preparation and Characterization of Fulleroid and Methanofullerene Derivatives. *J. Org. Chem.* **1995**, *60*, 532–538.

(17) Hoppe, H.; Sariciftci, N. S. J. Morphology of Polymer/Fullerene Bulk Heterojunction Solar Cells. *Mater. Chem.* **2006**, *16*, 45–61.

(18) Leach, S.; Vervloet, M.; Desprès, A.; Bréheret, E.; Hare, J. P.; Dennis, T. J.; Kroto, H. W.; Taylor, R.; Walton, D. R. M. Electronic-Spectra and Transitions of the Fullerene C_{60}. *Chem. Phys.* **1992**, *160*, 451–466.

(19) Gust, D.; Moore, T. A.; Moore, A. L. Solar Fuels via Artificial Photosynthesis. *Acc. Chem. Res.* **2009**, *42*, 1890–1898.

(20) Gust, D.; Moore, T. A.; Moore, A. L. Fullerenes Linked to Photosynthetic Pigments. *Res. Chem. Intermed.* **1997**, *23*, 621–651.

(21) Martín, N.; Sánchez, L.; Illescas, B.; Pérez, I. C_{60}-Based Electroactive Organofullerenes. *Chem. Rev.* **1998**, 2527–2547.

(22) Gómez, R.; Segura, J. L.; Martín, N. Highly Efficient Light-Harvesting Organofullerenes. *Org. Lett.* **2005**, *7*, 717–720.

(23) Hua, J.; Meng, F.; Ding, F.; Li, F.; Tian, H. Novel Soluble and Thermally-Stable Fullerene Dyad Containing Perylene. *J. Mater. Chem.* **2005**, *14*, 1849–1853.

(24) Shibano, Y.; Umeyama, T.; Matano, Y.; Tkachenko, N. V.; Lemmetyinen, H.; Araki, Y.; Ito, O.; Imahori, H. Large Reorganization Energy of Pyrrolidine-Substituted Perylenediimide in Electron Transfer. *J. Phys. Chem. C* **2007**, *111*, 6133–6142.

(25) Baffreau, J.; Leroy-Lhez, S.; Vân Anh, N.; Williams, R. M.; Hudhomme, P. Fullerene C_{60}-Perylene-3,4:9,10-bis(dicarboximide) Light-Harvesting Dyads: Spacer-Length and Bay-Substituent Effects on Intramolecular Singlet and Triplet Energy Transfer. *Chem.−Eur. J.* **2008**, *14*, 4974–4992.

(26) Kircher, T.; Löhmannsröben, H.-G. Photoinduced Charge Recombination Reactions of a Perylene Dye in Acetonitrile. *Phys. Chem. Chem. Phys.* **1999**, *1*, 3987–3992.

(27) Würthner, F. Perylene Bisimide Dyes as Versatile Building Blocks for Functional Supramolecular Architectures. *Chem. Commun.* **2004**, 1564–1579.

(28) Lang, E.; Würthner, F.; Köhler, J. Photophysical Properties of a Tetraphenoxy-Substituted Perylene Bisimide Derivative Characterized by Single-Molecule Spectroscopy. *ChemPhysChem* **2005**, *6*, 935–941.

(29) Lang, E.; Hildner, R.; Engelke, H.; Osswald, P.; Würthner, F.; Köhler, J. Comparison of the Photophysical Parameters for Three Perylene Bisimide Derivatives by Single-Molecule Spectroscopy. *ChemPhysChem* **2007**, *8*, 1487–1496.

(30) Magin, E. H.; Borsenberger, P. M. Electron-Transport in N, N′-bis(2-phenethyl)-perylene-3,4/9,10-bis(dicarboximide). *J. Appl. Phys.* **1993**, *73*, 787–791.

(31) Prathapan, S.; Yang, S. I.; Seth, J.; Miller, M. A.; Bocian, D. F.; Holten, D.; Lindsey, J. S. Synthesis and Excited-State Photodynamics of Perylene-Porphyrin Dyads. 1. Parallel Energy and Charge Transfer via a Diphenylethyne Linker. *J. Phys. Chem. B* **2001**, *105*, 8237–8248.

(32) Wicklein, A.; Lang, A.; Muth, M.; Thelakkat, M. Swallow-Tail Substituted Liquid Crystalline Perylene Bisimides: Synthesis and Thermotropic Properties. *J. Am. Chem. Soc.* **2009**, *131*, 14442–14453.

(33) Lee, H. J.; Yum, J.-H.; Leventis, H. C.; Zakeeruddin, S. M.; Haque, S. A.; Chen, P.; Seok, S. I.; Grätzel, M.; Nazeeruddin, Md. K. CdSe Quantum Dot-Sensitized Solar Cells Exceeding Efficiency 1% at Full-Sun Intensity. *J. Phys. Chem. C* **2008**, *112*, 11600–11608.

(34) Ford, W. E.; Kamat, P. V. Photochemistry of 3,4,9,10-Perylenetetracarboxylic Dianhydride Dyes. 3. Singlet and Triplet Excited-State Properties of the Bis(2,5-di-tert-butylphenyl)imide Derivative. *J. Phys. Chem.* **1987**, *91*, 6373–6380.

(35) Hofmann, C. C.; Bauer, P.; Haque, S. A.; Thelakkat, M.; Köhler, J. Energy- and Charge-Transfer Processes in Flexible Organic Donor-Acceptor Dyads. *J. Chem. Phys.* **2009**, *131*, 144512.

(36) Scharf, C.; Peter, K.; Bauer, P.; Jung, C.; Thelakkat, M.; Köhler, J. Towards the Characterization of Energy-Transfer Processes in Organic Donor-Acceptor Dyads Based on Triphenyldiamine and Perylenebisimides. *Chem. Phys.* **2006**, *328*, 403–409.

(37) Giaimo, J. M.; Lockard, J. V.; Sinks, L. E.; Scott, A. M.; Wilson, T. M.; Wasielewski, M. R. Excited Singlet States of Covalently Bound, Cofacial Dimers and Trimers of Perylene-3,4:9,10-bis(dicarboximide)s. *J. Phys. Chem. A* **2008**, *112*, 2322–2330.

(38) Hofkens, J.; Vosch, T.; Maus, M.; Köhn, F.; Cotlet, M.; Weil, T.; Herrmann, A.; Müllen, K.; De Schryver, F. C. Conformational Rearrangements in and Twisting of a Single Molecule. *Chem. Phys. Lett.* **2001**, *333*, 255–263.

(39) Ziessel, R.; Allen, B. D.; Rewinska, D. B.; Harriman, A. Selective Triplet-State Formation during Charge Recombination in a Fullerene/Bodipy Molecular Dyad (Bodipy = Borondipyrromethene). *Chem.−Eur. J.* **2009**, *15*, 7382–7393.

(40) Vosch, T.; Fron, E.; Hotta, J.-i.; Deres, A.; Uji-i, H.; Idrissi, A.; Yang, J.; Kim, D.; Puhl, L.; Haeuseler, A.; Müllen, K.; De Schryver, F. C.; Sliwa, M.; Hofkens, J. Synthesis, Ensemble and Single Molecule Characterization of a Diphenyl-Acetylene Linked Perylenediimide Trimer. *J. Phys. Chem. C* **2009**, *113*, 11773–11782.

(41) Oevering, H.; Paddon-Row, M. N.; Heppener, M.; Oliver, A. M.; Cotsaris, E.; Verhoeven, J. W.; Hush, N. S. Long-Range Photoinduced Through-Bond Electron-Transfer and Radiative Recombination via Rigid Nonconjugated Bridges - Distance and Solvent Dependence. *J. Am. Chem. Soc.* **1987**, *109*, 3258–3269.

(42) Weller, A. Photoinduced Electron-Transfer in Solution - Exciplex and Radical Ion-Pair Formation Free Enthalpies and Their Solvent Dependence. *Z. Phys. Chem.* **1982**, *133*, 93–98.

(43) Holman, M. W.; Liu, R.; Zang, L.; Yan, P.; DiBenedetto, S. A.; Bowers, R. D.; Adams, D. M. Studying and Switching Electron Transfer: From the Ensemble to the Single Molecule. *J. Am. Chem. Soc.* **2004**, *126*, 16126–16133.

(44) Veldman, D.; Chopin, S. M. A.; Meskers, S. C. J.; Janssen, R. A. J. Enhanced Intersystem Crossing via a High Energy Charge Transfer State in a Perylenediimide-Perylenemonoimide Dyad. *J. Phys. Chem. A* **2008**, *112*, 8617–8632.

(45) Marcus, R. A. On the Theory of Electron-Transfer Reactions. VI. Unified Treatment for Homogeneous and Electrode Reactions. *J. Chem. Phys.* **1965**, *43*, 679–701.

(46) Kestner, N. R.; Logan, J.; Jortner, J. Thermal Electron-Transfer Reactions in Polar-Solvents. *J. Phys. Chem.* **1974**, *78*, 2148–2166.

(47) Ulstrup, J.; Jortner, J. Effect of Intramolecular Quantum Modes on Free-Energy Relationships for Electron-Transfer Reactions. *J. Chem. Phys.* **1975**, *63*, 4358–4368.

(48) Jortner, J. Temperature-Dependent Activation-Energy for Electron-Transfer Between Biological Molecules. *J. Chem. Phys.* **1976**, *64*, 4860–4867.

(49) Barbara, P. F.; Meyer, T. J.; Ratner, M. A. Contemporary Issues in Electron Transfer Research. *J. Phys. Chem.* **1996**, *100*, 13148–13168.

(50) Imahori, H.; Hagiwara, K.; Akiyama, T.; Aoki, M.; Taniguchi, S.; Okada, T.; Shirakawa, M.; Sakata, Y. The Small Reorganization Energy of C_{60} in Electron Transfer. *Chem. Phys. Lett.* **1996**, *263*, 545–550.

(51) Gust, D.; Moore, T. A.; Moore, A. L. Photochemistry of Supramolecular Systems Containing C_{60}. *J. Photochem. Photobiol., B* **2000**, *58*, 63–71.

(52) Luo, C. P.; Fujitsuka, M.; Watanabe, A.; Ito, O.; Gan, L.; Huang, Y.; Huang, C. H. Substituent and Solvent Effects on Photoexcited States of Functionalized Fullerene[60]. *J. Chem. Soc., Faraday Trans.* **1998**, *84*, 527–532.

(53) Apperloo, J. J.; Martineau, C.; van Hal, P. A.; Roncali, J.; Janssen, R. A. J. Intra- and Intermolecular Photoinduced Energy and Electron Transfer Between Oligothienylenevinylenes and N-methylfulleropyrrolidine. *J. Phys. Chem. A* **2002**, *106*, 21–31.

(54) Anthony, S. M.; Bachilo, S. M.; Weisman, R. B. Comparative Photophysics of $C_{61}H_2$ Isomers. *J. Phys. Chem. A* **2003**, *107*, 10674–10679.

(55) Williams, R. M.; Zwier, J. M.; Verhoeven, J. W. Photoinduced Intramolecular Electron-Transfer in a Bridged C_{60} (Acceptor)-Aniline (Donor) System - Photophysical Properties of the First "Active" Fullerene Diad. *J. Am. Chem. Soc.* **1995**, *117*, 4093–4099.

(56) Ma, B.; Bunker, C. E.; Guduru, R.; Zhang, X.-F.; Sun, Y.-P. Quantitative Spectroscopic Studies of the Photoexcited State Properties of Methano- and Pyrrolidino-[60]Fullerene Derivatives. *J. Phys. Chem. A* **1997**, *101*, 5626–5632.

(57) Guldi, D. M.; Asmus, K.-D. Photophysical Properties of Mono- and Multiply-Functionalized Fullerene Derivatives. *J. Phys. Chem. A* **1997**, *101*, 1472–1481.

JP1035585